Chapter 5

Determining particulate – solid interphase strength using shear-induced anisotropy

(This paper is coauthored by Jianfeng Wang, Joseph E. Dove and Marte S. Gutierrez)
Dr. Joseph E. Dove is my major advisor and Dr. Marte S. Gutierrez is my co-advisor.

The resistance to shear deformation developed between a granular material layer in contact with a natural or manufactured material surface is critical to the stability of a variety of systems. By using discrete element method numerical simulations, we show that evolution of fabric and contact force anisotropy at the boundary between the surface and the granular media controls shear behavior. Full mobilization of granular material strength occurs when the contact force anisotropy developed at the interface is equal to the maximum contact force anisotropy of the granular media.

KEY WORDS: Interphase strength, Shear strength, Anisotropy, Dilatancy, Discrete analysis

5.1. Introduction

Determining the mechanisms responsible for quasistatic shear resistance within the interphase region between a granular material and a rough, continuous manufactured or natural material surface is of considerable importance to civil infrastructure engineering, geoscience, material science, geophysics and granular physics (Frost and Han 1999; Dove and Jarrett 2002; Uesugi and Kishida 1986; Jaeger et al. 1996). The interphase region consists of the surface with its asperities, and a variable thickness of granular material directly adjacent to the surface. The thickness of the granular portion of the interphase is normally associated with the thickness of the zone of intense shear (shear band), which can extend to about 10 to 14 median particle

diameters from the rough surface (Wang et al. 2005). Shear displacement of the continuous material with respect to the particles is resisted by the shear strength mobilized in the granular material within the interphase. The mechanisms by which the rough surface controls the mechanical behavior of the interphase region are not clearly understood. Without a basis for describing the strength of the interphase, general quantitative relationships such as failure criteria and constitutive equations are difficult to develop.

It is known that as surface roughness with respect to the particle diameter increases, particles within the interphase region experience increasing levels of both frictional interactions and dilation (Dove et al. 1997; Dove and Harping 1999) resulting in greater shear strength. However, it has proven difficult to relate surface roughness directly to shear strength (Kishida and Uesugi 1987; Jensen et al. 1999; Paikowsky and Xi 1997; Irsyam and Hryciw 1991; Hryciw and Irsyam 1993; Claquin and Emeriault 2001). Surfaces are characterized in terms of standardized statistical parameters, Fourier series, fractals and statistical functions. Each of these methods cannot provide a unique relationship with interphase strength because they represent an averaging or approximation of the surface that masks the geometric information at each particle to surface contact. This is further complicated when attempts are made to use discrete analyses requiring summation of particle to surface contact forces. Force summation yields correct results when applied to a single asperity because the ratio of shear stress (τ) to normal stress (σ) is proportional to the obliquity of the resultant force. Extending this concept to a general multi-asperity or random surface case is found to be problematic. This is because of nonlinearity in the superposition of forces acting on multiple asperities in all possible orientations.

Given the above constraints, the problem as addressed herein, is recast such that the shear-induced anisotropy of forces acting on the particles touching the rough surface is related to the mobilized shear strength of the system. The central thesis of this method is that the grains in direct contact with the surface control the degree to which internal shear resistance of the granular material can be mobilized. This notion leads directly to a study of the contacts at the surface using discrete methods. The statistical nature of the surface roughness relative to the particle sizes is implicitly incorporated in this approach with the discrete forces developed at the asperities preserved.

5.2. Methods

5.2.1. Numerical experiments

A two-dimensional discrete element model of a direct interface shear box (Wang et al. 2005) was created using the discrete code PFC2D (Itasca Consultants, Inc.). The device is formed by two fixed, rigid end boundaries, a bottom rough surface and a top boundary that applies normal stress through a servo mechanism [Figure 5.1(a)]. The rough surface consisted of regular or irregular triangular asperities, or of profiles made of actual material surfaces using a stylus profilometer. The lower surface is frictionless within 20 mm long regions from each shear box boundary. Quasi-static horizontal shear deformation (δ) is applied to the lower rough boundary [Figure 5.1(b)]. Discrete data are collected both in a 14 mm high sampling region and at the surface.

To systematically quantify the effects of surface geometry on the interphase strength behavior, five groups of numerical experiments in which geometry of surface asperities was varied were conducted. In Groups 1, 2 and 3, regular saw tooth asperities are used, with asperity height (R_t), asperity width (S_w) and spacing between asperities (S_r) varied in each group. Figure 5.2(a) shows the sketch of surface geometry for the regular saw tooth surfaces. The variables and constants in these three groups of experiments and their values tested are listed in Table 5.1. The asperity sizes are all normalized with respect to median particle diameter D_{50}, which has a constant value of 0.7 mm.

Table 5.1. Variables, constants of surface asperities and their values used in the Experimental Groups 1, 2 and 3.

Group	Variable	Values of Variables	R_t/D_{50}	S_r/D_{50}	S_w/D_{50}
1	R_t/D_{50}	0.1, 0.2, 0.5, 1, 1.2, 1.5, 2, 3, 5	Varied	0	2
2	S_r/D_{50}	0.2, 0.5, 1, 2, 3, 5, 8, 10	1	Varied	2
3	S_w/D_{50}	0.2, 0.5, 1, 2, 3, 4, 5, 10	1	0	Varied

In the fourth group of experiments, irregular saw tooth asperities are generated randomly to investigate how irregular surfaces affect the interphase behavior. Three parameters, namely asperity unit (A_u), asperity ratio (A_r) and maximum accumulated asperity height (R_{tmax}), are introduced for irregular surfaces to give varying degrees of roughness. Figure 5.2(b) is a sketch

of irregular surface asperities. Asperity unit is the unit segment length of the projection of any linear asperity segment in the horizontal direction; asperity ratio is the ratio of the unit segment length of the projection of any linear asperity segment in the vertical direction to that in the horizontal direction; and maximum accumulated asperity height is the prescribed maximum elevation difference between the peak and the valley of the whole surface. Asperity unit and maximum accumulated asperity height are also normalized with respect to median particle diameter. To form the surface a random number multiplier is applied to the unit segment length in both horizontal and vertical directions using the values of A_u and A_r as starting values. Approximate control of the surface geometry, and thus different roughness degrees of irregular surfaces can be obtained by assigning different values to the above three parameters. Their values used in seven numerical experiments in Group 4 are listed in Table 5.2.

Table 5.2. Values of A_u, A_r and R_{tmax} used in Experimental Group 4.

Variable	Numerical Experiment						
	A	B	C	D	E	F	G
A_u/D_{50}	1	2	2	4	2	4	4
A_r	1	1	0.5	2	0.25	0.25	4
R_{tmax}/D_{50}	2	2	2	4	1	2	4

In Group 5, two-dimensional profiles of three manufactured geomembrane surfaces, wood, stone and concrete are used. Digital profile data collected with a stylus profilometer at a 1μm data point spacing along the surfaces (Figure 5.3) are used to create the lower boundary in PFC2D.

For all experiments, two sets of granular samples, one of uniformly graded (mono-dispersed) material and the other of well graded (poly-dispersed) material are used to evaluate the effects of particle-size distribution on the interphase behavior. The maximum and minimum particle diameter (D_{max}, D_{min}) is 0.735 mm and 0.665 mm respectively, for the uniformly graded material, and 1.05 mm and 0.35 mm respectively, for the well graded material. The grain to surface friction coefficient ($\tan\phi_\mu$) is 0.05 for all the experiments. A separate series of numerical experiments were conducted with well-graded material. Additional grain to surface friction

coefficient values of 0.2 and 0.5 were used to determine how this variable affects the interphase strength behavior.

The Hertz-Mindlin contact model was implemented in all the simulations. An additional particle rolling resistance model was applied at both particle-particle contacts and particle-boundary contacts (Wang et al. 2004). Physical constants used in the simulations include: Particle density 2650 kg/m^3; shear modulus and Poisson's ratio of the particles, 29 GPa and 0.3 respectively; critical normal and shear viscous damping coefficient, both equal to 1.0; time step 5.0×10^{-5} sec; and interparticle and particle-boundary friction coefficient during shear, 0.5 and 0.9 respectively.

5.2.2. Calculation of anisotropy parameters and principal directions

We employ the concept of shear-induced anisotropies of fabric and contact forces and their spatial correlations (Rothenburg 1980; Bathurst and Rothenburg 1990; Rothenburg and Selvadurai 1981; Christoffersen et al. 1981; Majmudar and Behringer 2005) to homogenize the discrete data into a useable form. Anisotropy, as used herein, refers to the deviation of the contact and contact force orientations from an initial state due to shearing. The use of fabric and contact force anisotropy provides quantitative information on how the particle to particle and particle to surface contacts and their magnitudes are spatially distributed inside the granular material.

The two-dimensional, second order density distribution tensors (Rothenburg 1980) are used to describe the anisotropy of fabric and contact forces both in the granular assemblage and for the particles touching the surface. These tensors are computed from the discrete simulation data and are defined as follows:

$$F_{ij} = \int_0^{2\pi} E(\theta) n_i n_j d\theta = \frac{1}{N_c}\sum_{k=1}^{N_c} n_i^k n_j^k \,, \tag{5-1}$$

$$N_{ij} = \frac{1}{2\pi}\int_0^{2\pi} \frac{\bar{f}_n(\theta)}{\bar{\bar{f}}_0} n_i n_j d\theta = \frac{1}{N_c}\sum_{k=1}^{N_c} \frac{f_n^k}{\bar{\bar{f}}_0} n_i^k n_j^k \,, \tag{5-2}$$

$$S_{ij} = \frac{1}{2\pi}\int_0^{2\pi} \frac{\bar{f}_s(\theta)}{\bar{\bar{f}}_0} t_i n_j d\theta = \frac{1}{N_c}\sum_{k=1}^{N_c} \frac{f_s^k}{\bar{\bar{f}}_0} t_i^k n_j^k \,, \tag{5-3}$$

where, F_{ij}, N_{ij} and S_{ij} are fabric, average contact normal force and average contact shear force tensors, respectively; $E(\theta)$, $\bar{f}_n(\theta)$ and $\bar{f}_s(\theta)$ are the corresponding density distribution functions; f_n^k and f_s^k are contact normal force and shear force, respectively; $\boldsymbol{n}=(\cos\theta,\sin\theta)$ is unit contact normal vector, and $\boldsymbol{t}=(-\sin\theta,\cos\theta)$ is the vector perpendicular to $\boldsymbol{n}$; and N_c is the total number of contacts in the volume. $\bar{f}_0$ is the average contact normal force calculated by:

$$\bar{f}_0=\frac{1}{2\pi}\int_0^{2\pi}\bar{f}_n(\theta)d\theta=\frac{1}{N_c}\sum_{k=1}^{N_c}f_n^k\,. \tag{5-4}$$

Magnitudes of contact forces and contact normals within a sheared granular assemblage demonstrate periodicity with respect to measurement orientation (Majmudar and Behringer 2005). The following second order Fourier series expressions for $E(\theta)$, $\bar{f}_n(\theta)$ and $\bar{f}_s(\theta)$ were proposed by Bathurst et al. 1991 to fit the numerical simulation data:

$$E(\theta)=\frac{1}{2\pi}\left[1+a\cos 2(\theta-\theta_a)\right], \tag{5-5}$$

$$\bar{f}_n(\theta)=\bar{f}_0\left[1+a_n\cos 2(\theta-\theta_n)\right], \tag{5-6}$$

and

$$\bar{f}_s(\theta)=\bar{f}_0\left[a_w-a_s\sin 2(\theta-\theta_s)\right]. \tag{5-7}$$

In these equations, a, a_n, a_s and a_w are the coefficients of contact normal, contact normal force and contact shear force anisotropies, respectively; and θ_a, θ_n and θ_s are the principal directions of contact normal, contact normal force and contact shear force, respectively. These anisotropy parameters are invariant quantities of the second order tensors defined in Equations (5-1) to (5-3) above. Particularly, a, a_n, a_s and a_w are related to the eigenvalues of tensor F_{ij}, N_{ij} and S_{ij}, respectively; and θ_a, θ_n and θ_s are the eigenvectors of these tensors.

The average contact resultant force tensor, R_{ij}, is defined as:

$$R_{ij}=\frac{1}{2\pi}\int_0^{2\pi}\frac{\bar{f}_r(\theta)}{\bar{f}_{r0}}m_i m_j d\theta=\frac{1}{N_c}\sum_{k=1}^{N_c}\frac{f_r^k}{\bar{f}_{r0}}m_i^k m_j^k\,. \tag{5-8}$$

$\bar{f}_r(\theta)$ is the average contact resultant force density distribution function; f_r is the contact resultant force; and, $\boldsymbol{m} = (\cos\alpha, \sin\alpha)$ is the unit vector in the direction of contact resultant force. $\bar{f}_{r0}$ is the average contact resultant force calculated from:

$$\bar{f}_{r0} = \frac{1}{2\pi}\int_0^{2\pi} \bar{f}_r(\theta) d\theta = \frac{1}{N_c}\sum_{k=1}^{N_c} f_r^k \,. \tag{5-9}$$

The Fourier series approximation for $\bar{f}_r(\theta)$ is written as:

$$\bar{f}_r(\theta) = \bar{f}_{r0}\left[1 + a_r \cos 2(\theta - \theta_r)\right], \tag{5-10}$$

where a_r and θ_r are the coefficient and principal direction (eigenvector) of the contact resultant force anisotropy.

Physically, θ_n reflects the statistics of the relative particle to surface geometry and θ_r accounts for both surface roughness and friction. They are expressed as angular deviations of the principal directions from vertical.

5.2.3. Average stress components

The ratio of shear stress to normal stress (τ/σ) is determined at peak state by using a force summation over the asperities at the rough surface. The average stress ratio $(\tau/\sigma)_{ave}$ in the 14 mm high sampling region [Figure 5.1(a)] within the granular assemblage is also computed from the average stress tensor defined as (Rothenburg and Selvadurai 1981; Christoffersen et al. 1981):

$$\sigma_{ij} = \frac{1}{V}\sum_{k=1}^{N_c} f_i^k l_j^k \,. \tag{5-11}$$

f_i^k is the contact force acting at the *k*-th contact point between the two particles; l_j^k is the branch vector connecting the centroids of two particles forming the *k*-th contact point. A contact is created only when it transmits contact forces, $\boldsymbol{f}$.

The average stress components acting on a plane can be expressed in terms of anisotropy parameters as follows:

$$\sigma_{11} = p\left[1+\frac{a\cdot a_n}{2}\cos 2(\theta_a-\theta_n)+\frac{1}{2}\left(a\cos(2\theta_a)+a_n\cos(2\theta_n)+a_s\cos(2\theta_s)\right)-\frac{a\cdot a_w}{2}\sin(2\theta_a)\right], \quad (5\text{-}12)$$

$$\sigma_{22} = p\left[1+\frac{a\cdot a_n}{2}\cos 2(\theta_a-\theta_n)-\frac{1}{2}\left(a\cos(2\theta_a)+a_n\cos(2\theta_n)+a_s\cos(2\theta_s)\right)+\frac{a\cdot a_w}{2}\sin(2\theta_a)\right], \quad (5\text{-}13)$$

$$\sigma_{12} = \sigma_{21} = p\left[\frac{1}{2}\left(a\sin(2\theta_a)+a_n\sin(2\theta_n)+a_s\sin(2\theta_s)\right)+\frac{a\cdot a_w}{2}\cos(2\theta_a)\right]. \quad (5\text{-}14)$$

where $p=\frac{m_v\bar{l}_0\bar{f}_0}{2}$, in which, m_v is the contact density and $\bar{l}_0$ is the average contact vector length over the volume. These equations are used for mono-dispersed granular assemblages where $\bar{l}_0$ is constant.

5.3. Results

5.3.1. Control of contact force anisotropy on interphase strength

Anisotropy at the interface is dominated by the particle to surface contact. Therefore the principal force orientations, θ_r and θ_n, used herein are based on the contacts and friction coefficient between the particles and rough surface. In contrast, principal directions computed within the 14 mm high sampling region differ from those computed at the interface because of the more complex but complete force system acting on the particles. In this region, the effects of vertical, horizontal and shear forces act over the region and θ_r corresponds to the major principal stress direction.

When the inclusion surface is displaced in shear with respect to the granular assemblage, the surface asperities interact directly with the particles touching the surface. Macroscale stress versus displacement relations measured on the lower surface of the device and within the 14 mm high sampling region during shear simulations displayed post-peak stress displacement-softening followed by a steady state of shear at large deformations. Dilation was observed with the highest dilation rate occurring at peak state, which then diminished as steady state was reached. At the grain scale, contact forces resisting displacement of the rough surface develop and extend into the granular mass. Force chains develop to resist shear [Figure 5.1(b)] and disperse the contact forces from the surface into the granular assemblage. It has been shown (Majmudar and Behringer 2005) that long-range force correlations parallel to the force chains extend for

approximately 15 particle diameters but dissipate within 2 to 3 particle diameters in directions perpendicular to the force chains. Anisotropies of average contact normal force, shear force and resultant force grow rapidly after shearing begins, and reach their maximum at peak state. Fabric (contact normal) anisotropy increases as coordination number decreases during shear.

The shear strength of the system depends on the capacity of the surface to support development of anisotropy of fabric and contact forces (Bathurst and Rothenburg 1990). The greatest strength that can be achieved, the strength of the granular assemblage, is reached when the surface develops anisotropy of similar magnitude as that of the granular material. In other words, if the surface mimics, in terms of anisotropy, a layer of particles instead of a solid surface, the full strength of the granular material will be mobilized.

Figure 5.4 contains polar distributions of contact normal, contact normal force and contact resultant force at peak stress state for a surface with 45-degree triangular asperities having height equal to the median particle diameter, and a surface with randomly generated asperity geometry. In Figure 5.4, since only contacts and contact forces at the lower boundary between particles and the surface are shown, they are all distributed in the third and fourth quadrant. It can be seen that for both cases, only the particle to surface contacts in the fourth quadrant are working effectively to sustain the contact force chains. As a result, the contact normal forces and resultant forces are predominantly confined to the fourth quadrant as forces are transferred to the particles by the advancing asperities.

In contrast to the regular surface [(Figure 5.4(a)], the randomly generated surface [Figure 5.4(b)] has a larger percentage of its surface that is nearly horizontal. Accordingly, the contact normal distribution is located around the vertical direction. The values of principal directions θ_n and θ_r are 23 degrees and 26 degrees respectively, for the randomly generated surface, which are lower than the values, 42 degrees and 41 degrees respectively, for the regular surface. Meanwhile, the randomly generated surface has lower mobilized shear strength than that of the regular surface.

Figure 5.5 relates stress ratio (τ/σ) at peak state measured at the surface to θ_n and θ_r computed for the first row of particles touching the rough surface. The peak stress ratio measured from a simulated direct shear test on the same granular material alone (no surface) is 0.63. This is also the maximum possible strength that can be achieved by an interphase system.

The strength ratio mobilized by a given surface increases linearly with θ_n and θ_r, reaches an upper limit at about 30 degrees and then remains nearly constant thereafter. This upper limit reflects the strength ratio of the granular material itself. When these data are written in terms of θ_r, the sloping linear portion of the curve passes through the origin, which corresponds to a surface with no roughness. However, when written in terms of θ_n, the vertical axis intercept is equal to the interface friction coefficient ($\tan\phi_\mu$). These results in terms of θ_n and θ_r are identical in form for τ/σ and $(\tau/\sigma)_{ave}$, indicating that results observed for anisotropy computed at the surface applies to shear zones away from the surface. Surface asperities allow growth and propagation of force chains into the granular mass. Force chains cause intense shear of the particles with respect to one another and give rise to shear bands. The results are also identical for monodisperse particle systems except that the maximum mobilized shear strength is lower than that of the polydisperse material.

5.3.2. Effects of particle to surface friction

The influence of particle to surface friction is shown in Figures 5.5(a) and 5.5(c). For $\tan\phi_\mu$ of 0.05 and 0.2, the effect of surface geometry is the same. However, for the high interface friction case (0.5), the force required to displace the particles increases. The magnitude of this increase depends on the surface geometry (Figure 5.6). It is found that for a surface with regular triangular asperities, sliding of the particles occurs over the surface regardless of ϕ_μ. However, for irregular surfaces and real material surfaces, the degree of interface friction mobilization is lower because a larger proportion of particles are entrapped in the valleys of the asperities and cannot move.

Figure 5.7 shows the relationship between θ_n and θ_r in different interface friction cases. As ϕ_μ increases, the degree of interface friction mobilization at the surface decreases. When ϕ_μ = 2.8 degrees, θ_n is about 3 degrees less than θ_r for all the surfaces. This means that friction at the surface is fully mobilized at peak state. When ϕ_μ = 11.3 degrees, the difference between θ_n and θ_r is approximately equal to ϕ_μ for surfaces that have asperities unable to fully mobilize the interface strength ($\theta_r \leq 30$ degrees). When $\theta_r > 30$ degrees, the difference between θ_n and

θ_r becomes insignificant because the asperities engage the surface particles and prevent them from moving. When ϕ_μ = 26.5 degrees, the difference between θ_n and θ_r is smaller than the interface friction angle for most surfaces, and becomes negligible when $\theta_r > 40$ degrees.

When θ_n and θ_r are greater than about 30 degrees the surface is sufficiently rough to fully mobilize the granular material shear strength regardless of the particle to surface friction coefficient (Figure 5.5). A larger variation in the maximum mobilized interface strength is observed when the particle-surface friction is high (0.5). The upper and lower bounds of the data are established by regular, triangular 'saw tooth' surfaces and randomly generated irregular surfaces, respectively. The difference between the upper and lower bound values is approximately 15 percent to 20 percent of the granular material strength. This difference is caused by a greater percentage of the contact force distribution lying in the third quadrant due to varying asperity slopes on the irregular surfaces. We have found that if finite contact resultant forces are located in the third quadrant, they will oppose motion and lead to a reduction of the total strength ratio when horizontal forces are summed.

It must be noted that θ_n and θ_r are not direct measures of the inclusion surface roughness. Instead, they are results of mechanical interaction between the surface asperities and granular media and thus implicitly reflect the important consequences of relative particle to surface geometry. In general, greater relative particle-surface roughness and friction coefficient result in greater θ_n, θ_r and mobilized interface strength. This approach is independent of statistical surface roughness parameters and suggests that the problem is one of contact and is not purely geometrical as past research presumed (Dove and Jarrett 2002; Uesugi and Kishida 1986; Kishida and Uesugi 1987).

5.4. Conclusions

A new approach to the problem of granular material strength mobilization adjacent to a rough continuous surface was presented. By extracting discrete data from the particle to surface contacts, the control of surface roughness on interphase strength mobilization can be clearly demonstrated and quantified. The results presented in this paper are for spherical particles in a dense initial packing. We anticipate that the methodology presented herein is general for any grain shape and initial porosity but the slopes of the curves in Figure 5.5 will likely be different.

Laboratory interface shear test results for subrounded, polydisperse particles agree with these simulation data.

Acknowledgements

This material is based upon work supported by the National Science Foundation under Grant No. CMS-0200949. Any opinions, findings, and conclusions or recommendations expressed in this material are those of the authors and do not necessarily reflect the views of the National Science Foundation.

Notation

The following symbols are used in this paper:

a = second order coefficient of contact normal anisotropy

a_n = second order coefficient of average contact normal force anisotropy

a_s, a_w = second order coefficient of average contact shear force anisotropy

A_u = asperity unit

A_r = asperity ratio

D_{50} = median particle diameter (mm)

D_{max} = maximum particle diameter (mm)

D_{min} = minimum particle diameter (mm)

E = efficiency parameter

$\boldsymbol{f}$ = contact force vector

$\bar{f}_0$ = average contact normal force

f_n, f_s = contact normal force and shear force

$\bar{f}_n(\theta)$ = density distribution function of average contact normal force

$\bar{f}_s(\theta)$ = density distribution function of average contact shear force

F_{ij} = second order density distribution tensor of fabric

$\boldsymbol{l}$ = branch vector

$\bar{l}_0$ = assembly average contact vector length

$\bar{l}(\theta)$ = distribution of contact vector length

$m_v = N_c/V$, contact density

$\boldsymbol{n}$ = unit contact normal vector

N_c = total number of contacts

N_{ij} = second order density distribution tensor of average contact normal force

N_p = total number of particles within the volume

r = radius of particle

R_t = asperity height (mm)

R_{tave} = average value of maximum asperity height over a series of assessment lengths, L (mm)

R_{tmax} = maximum accumulated asperity height (mm)

s = mean stress, $(\sigma_1 + \sigma_2)/2$

S_{ij} = second order density distribution tensor of average contact shear force

S_r = spacing between asperities (mm)

S_w = asperity width (mm)

t = deviator stress, $(\sigma_1 - \sigma_2)/2$

$\boldsymbol{t}$ = unit contact tangent vector

δ = horizontal shear deformation

ϕ_μ = particle-surface friction angle (degrees)

θ_a = principal direction of contact normal anisotropy (degrees)

θ_n = principal direction of average contact normal force anisotropy (degrees)

θ_r = principal direction of average contact resultant force anisotropy (degrees)

θ_s = second order principal direction of average contact shear force anisotropy

σ = normal stress

σ_{ij} = stress tensor

τ = shear stress

References

Bathurst, R.J., and Rothenburg, L (1990), "Observation on Stress-Force-Fabric Relationships in Idealized Granular Materials," Mechanics of Materials, 9, 65-80.

Christoffersen, J., Mehrabadi, M.M. and Nemat-Nasser, S (1981), "A Micro-mechanical Description of Granular Material Behavior," J. Appl. Mech, 48, ASME, 339-344.

Claquin, C., and Emeriault, F (2001), "Interface Behavior of Granular Materials: Discrete Numerical Simulation and Statistical Homogenization," Powders & Grains 2001, Kishino, ed., Swets & Zeitlinger, Lisse, 323-326.

Dove, J.E., Frost, J.D., Bachus, R.C., and Han, J (1997), "The Influence of Geomembrane Surface Roughness on Interface Strength," Proceedings of Geosynthetics '97 Conference, Vol. 2, 863-876.

Dove, J.E., and Jarrett, J.B (2002), "Behavior of Dilative Sand Interface in a Geotribology Framework," Journal of Geotechnical and Geoenvironmental Engineering, 128(1), 25-37.

Dove, J.E., and Harping, J.C (1999), "Geometric and Spatial Parameters for Analysis of Geomembrane/Soil Interface Behavior," Proceeding of Geosynthetics, Boston, MA, International Fabrics Association International, Vol. 1, 575-588.

Frost, J.D., and Han, J (1999), "Behavior of Interfaces between Fiber-Reinforced Polymers and Sands," Journal of Geotechnical and Geoenvironmental Engineering, 125(8), 633-640.

Hryciw, R.D., and Irsyam, M (1993), "Behavior of Sand Particles Around Rigid Ribbed Inclusions During Shear," Soils and Foundations, 33(3), 1-13.

Irsyam, M., and Hryciw, R.D (1991), "Frictional and Passive Resistance in Soil Reinforced by Plane Ribbed Inclusions," Géotechnique, 41(4), 485-498.

Jaeger, H.M., Nagel, S.R., and Behringer, R.P (1996), "Granular Solids, Liquids, and Gases," Rev. Mod. Phys. 68, 1259-1273.

Jensen, R.P., Bosscher, P.J., Plesha, M.E., and Edil, T.B (1999), "DEM Simulation of Granular Media --- Structure Interface: Effects of Structure Roughness and Particle Shape," International Journal for Numerical and Analytical Methods, 23, 531-547.

Kishida, H., and Uesugi, M (1987), "Tests of Interface between Sand and Steel in the Simple Shear Apparatus," Géotechnique, 37(1), 45-52.

Majmudar T. S., Behringer R. P.: "Contact force measurements and stress-induced anisotropy in granular materials." Nature, 435, 1079 (2005)

Paikowsky, S.G., and Xi, F (1997), "Photoelastic Quantitative Study of the Behavior of Discrete Materials with Application to the Problem of Interfacial Friction," Research Report, Air Force Office of Scientific Research, Research Grant F49620-93-0267.

Rothenburg L.: “Micromechanics of idealized granular system.” Ph.D. Dissertation, Carleton University, Ottawa, Ontario, Canada (1980)

Rothenburg, L., and Selvadurai, A.P.S (1981), “A Micromechanical Definition of the Cauchy Stress Tensor for Particulate Media,” Procs. Int. Symp. on the Mechanical Behavior of Structured Media, (ed Selvadurai), Ottawa, Part B, 469-486.

Uesugi, M., and Kishida, H (1986), “Influential Factors of Friction between Steel and Dry Sands,” Soils and Foundations, 26(2), 33-46.

Uesugi, M., and Kishida, H (1986), “Frictional Resistance at Yield between Dry Sand and Mild Steel,” Soils and Foundations, 26(4), 139-149.

Wang, J.F., Dove, J.E., Gutierrez, M.S., and Corton, J.D (2005), “Shear Deformation in the Interphase Region,” Powders and Grains 2005 (R. Garcia-Rojo, H.J. Herrmann, S. McNamara, Eds), Stuttgart, Germany, 747-750.

Wang, J.F., Gutierrez, M.S., and Dove, J.E (2005), “Strain Localization in an Idealized Interphase System,” Proc. 2005 Joint ASME/ASCE/SES Conf. Mech. Mat., Baton Rouge, Louisiana.

Wang, J.F., Gutierrez, M.S., and Dove, J.E (2004), “Effect of Particle Rolling Resistance on Interface Shear Behavior,” Proceedings 17th ASCE Engineering Mechanics Conference, Newark, Delaware, 56-63.

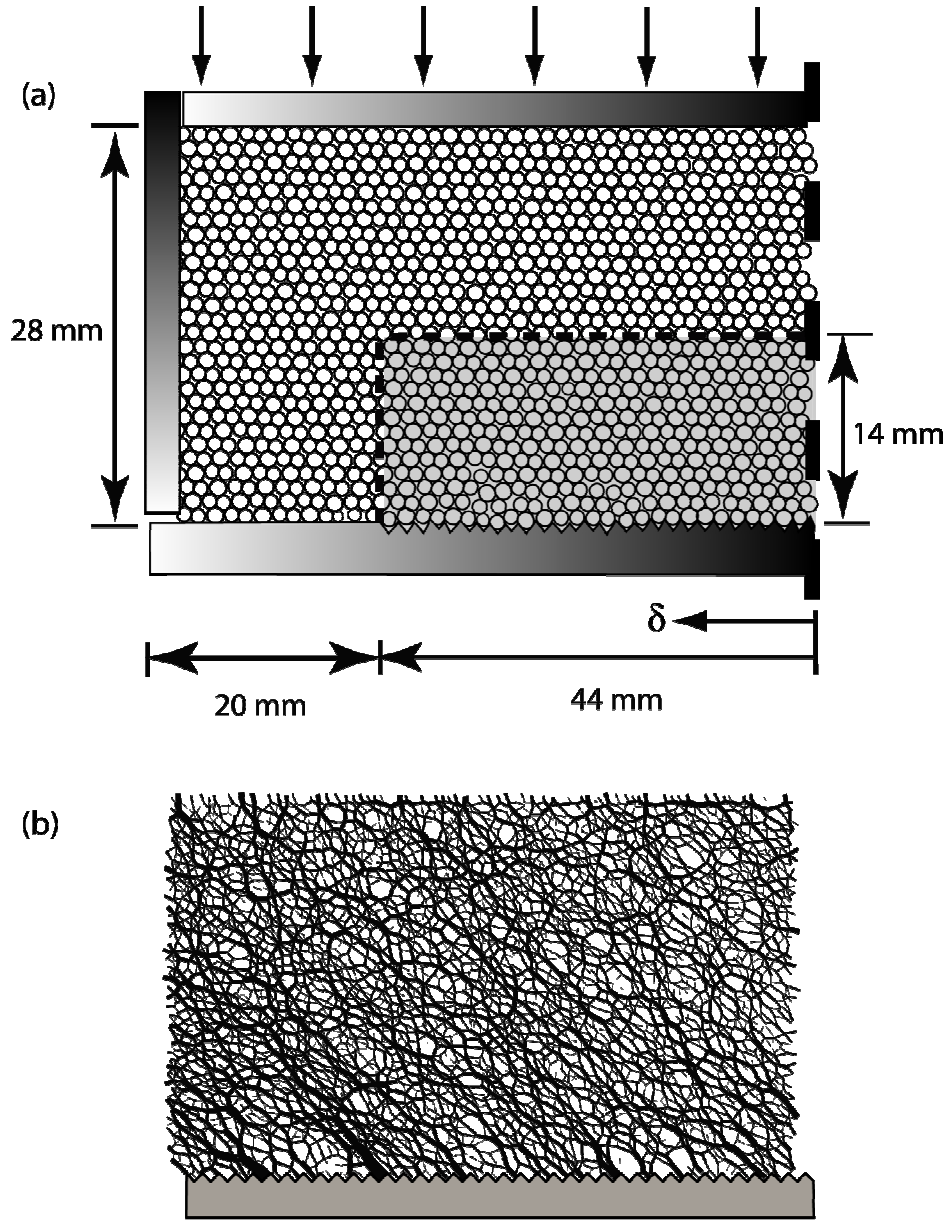

Figure 5.1. (a) Sketch of 2D simulation direct interface shear box (left half only); (b) Force chain network within the entire shear box at peak stress state for a regular roughened surface with 45-degree asperity slopes and asperity height to median particle diameter ratio (R_f/D) of 1.0.

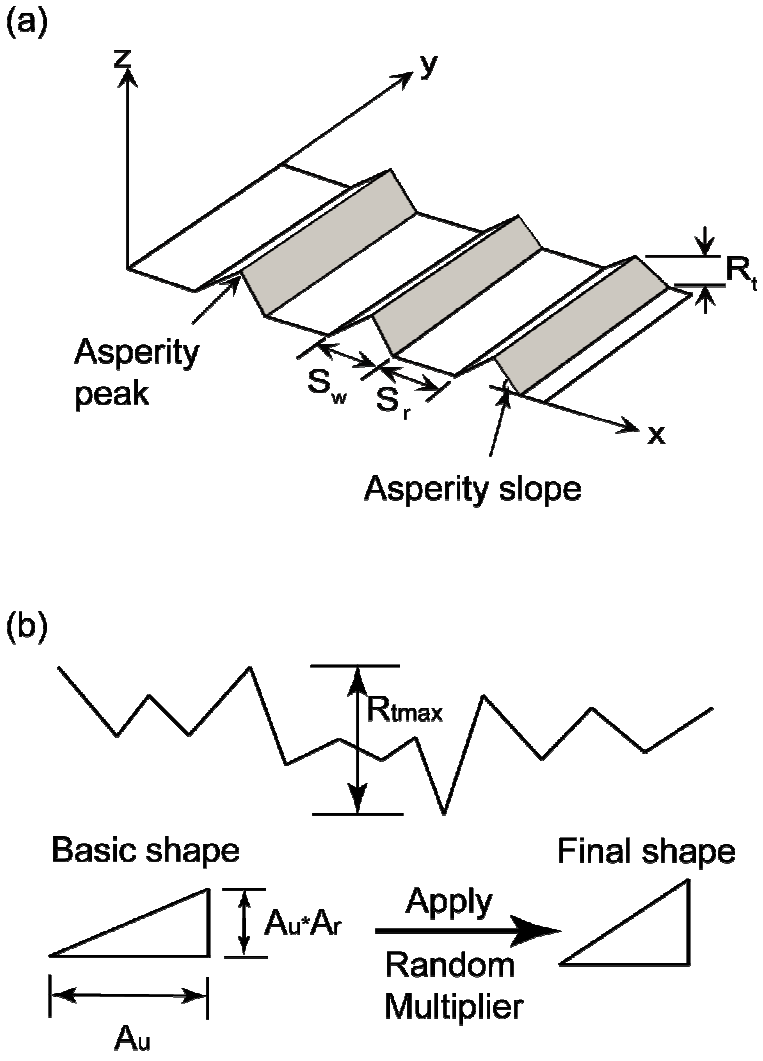

Figure 5.2. Sketches for regular and irregular triangular surface asperities: (a) For a regular triangular asperity, the geometry is determined by three parameters, R_t, S_w and S_r; (b) The basic shape of an irregular triangular surface asperity is "unit asperity segment" defined by A_u and A_r.

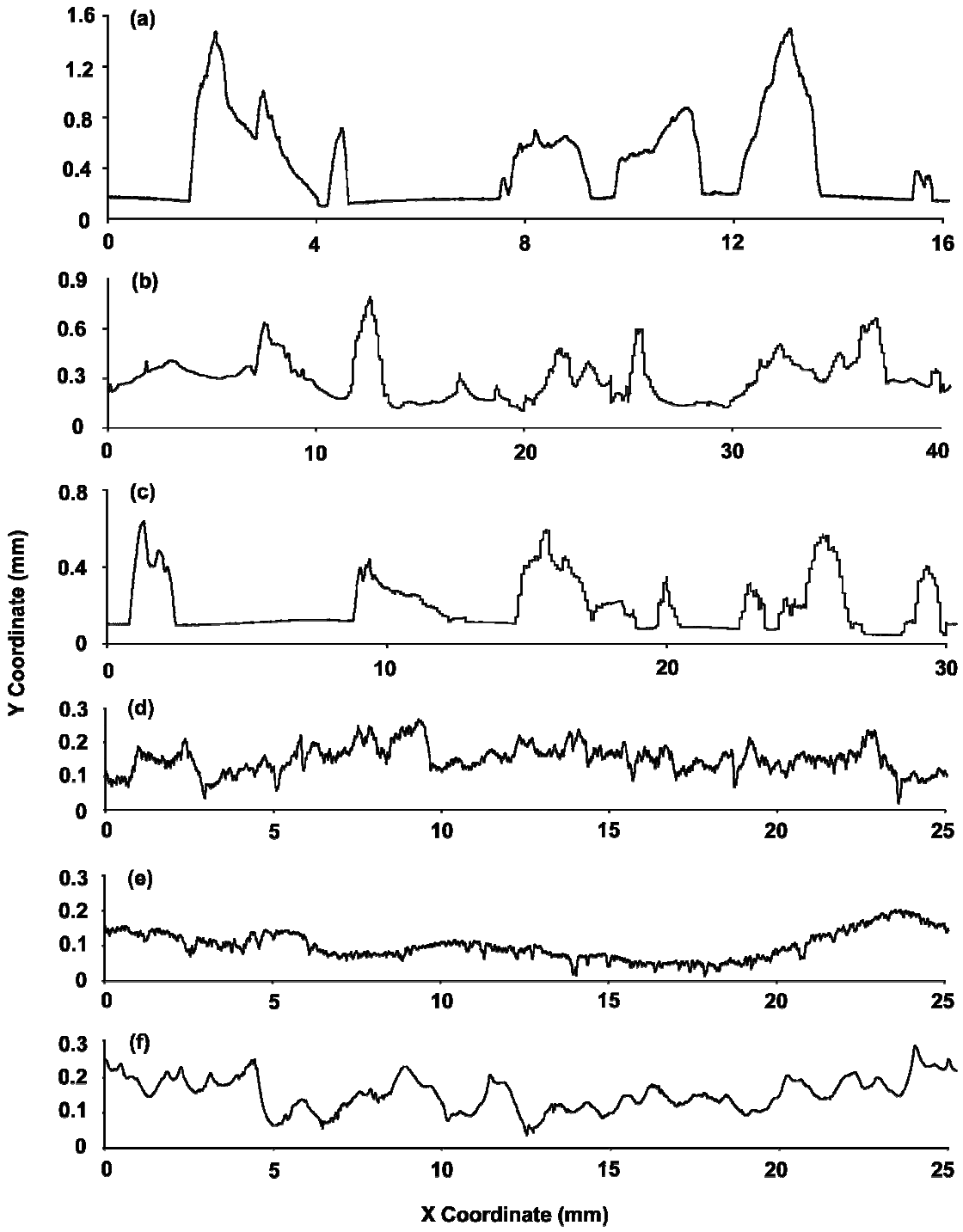

Figure 5.3. Surface profiles of manufactured and natural surfaces used in this study: (a) High Density Polyethylene textured geomembrane surface No. 1; (b) High Density Polyethylene textured geomembrane surface No. 2; (c) High Density Polyethylene textured geomembrane surface No. 3; (d) Wood surface; (e) Stone surface; (f) Concrete surface. Polymer surfaces were manufactured using a coextrusion process.

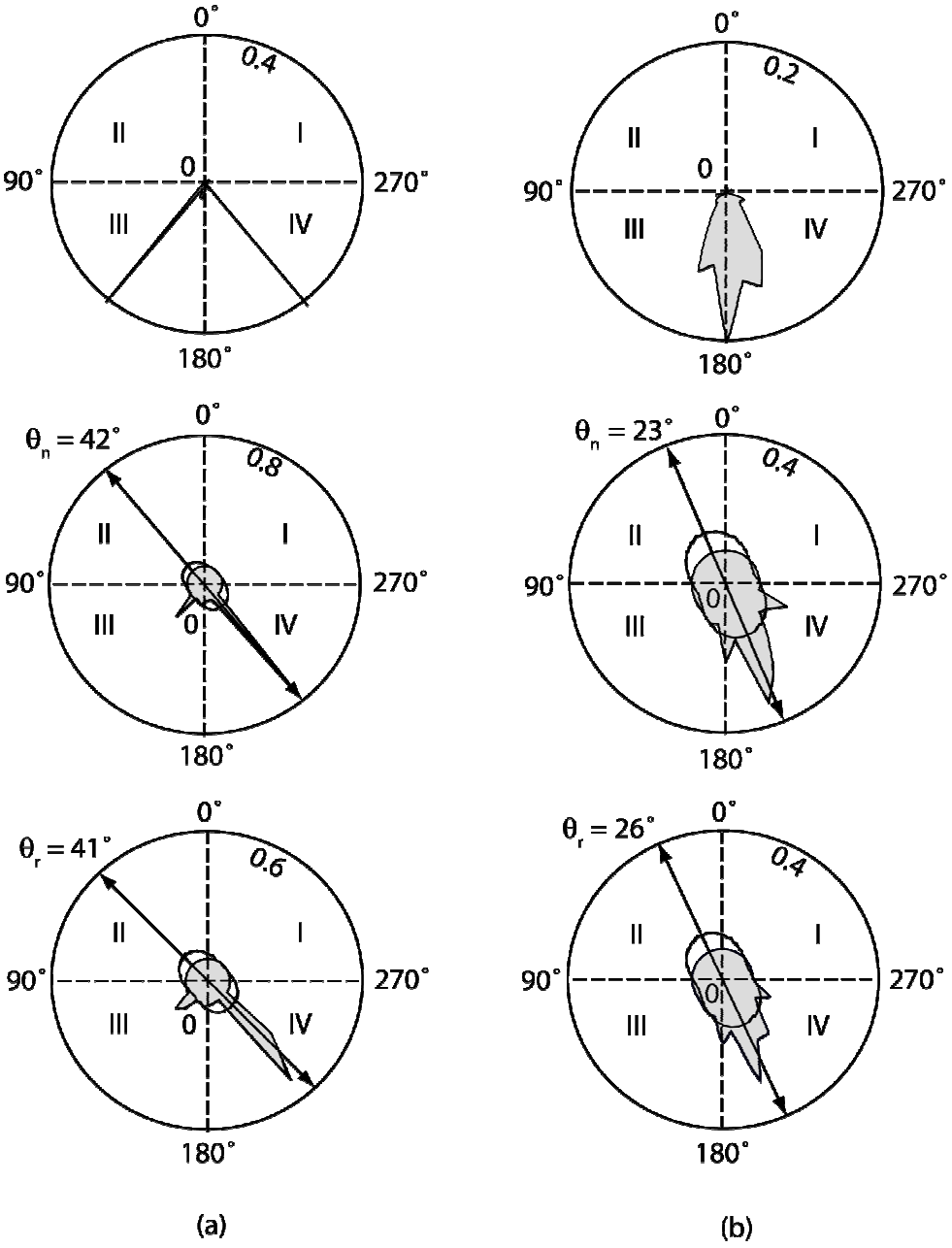

Figure 5.4. Polar distributions of anisotropy and principal directions for the first row of particles touching the surface with $\tan\phi_\mu = 0.05$. Top – contact normal, middle – contact normal force, bottom – contact resultant force. Roman numerals identify quadrants. Shaded areas are the density distributions and the unshaded areas are the Fourier series approximations to the density distributions. Arrows indicate principal directions. (a) regular triangular asperities with 45-degree slope and asperity height to median particle diameter ratio of 1.0; (b) Randomly generated surface.

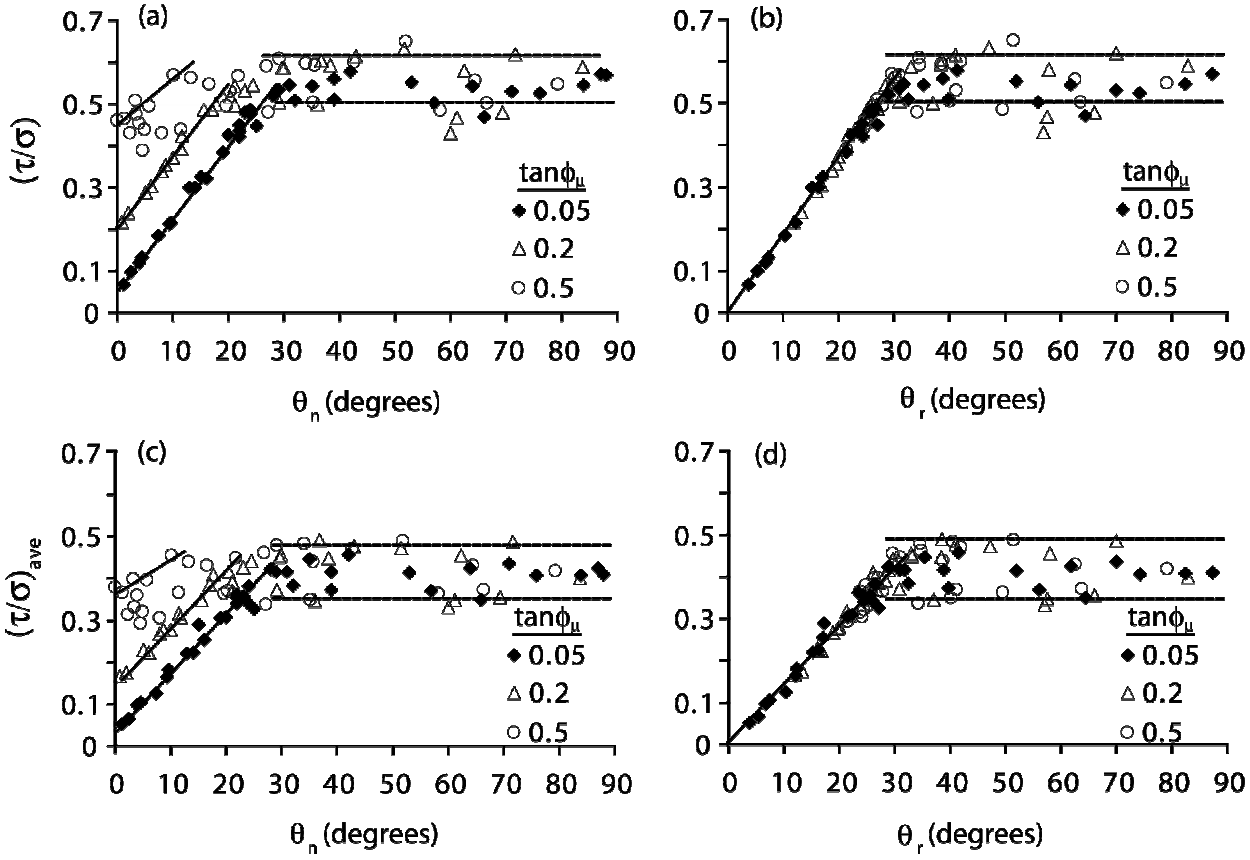

Figure 5.5. Control of principal directions of contact normal force (θ_n) and resultant force anisotropy (θ_r) on peak stress ratio: (a) and (b) peak stress ratios measured at the surface (τ/σ); (c) and (d) average stress ratio measured in the sampling region, $(\tau/\sigma)_{ave}$. The figures indicate that the same mechanism controls stress ratio regardless of measurement location.

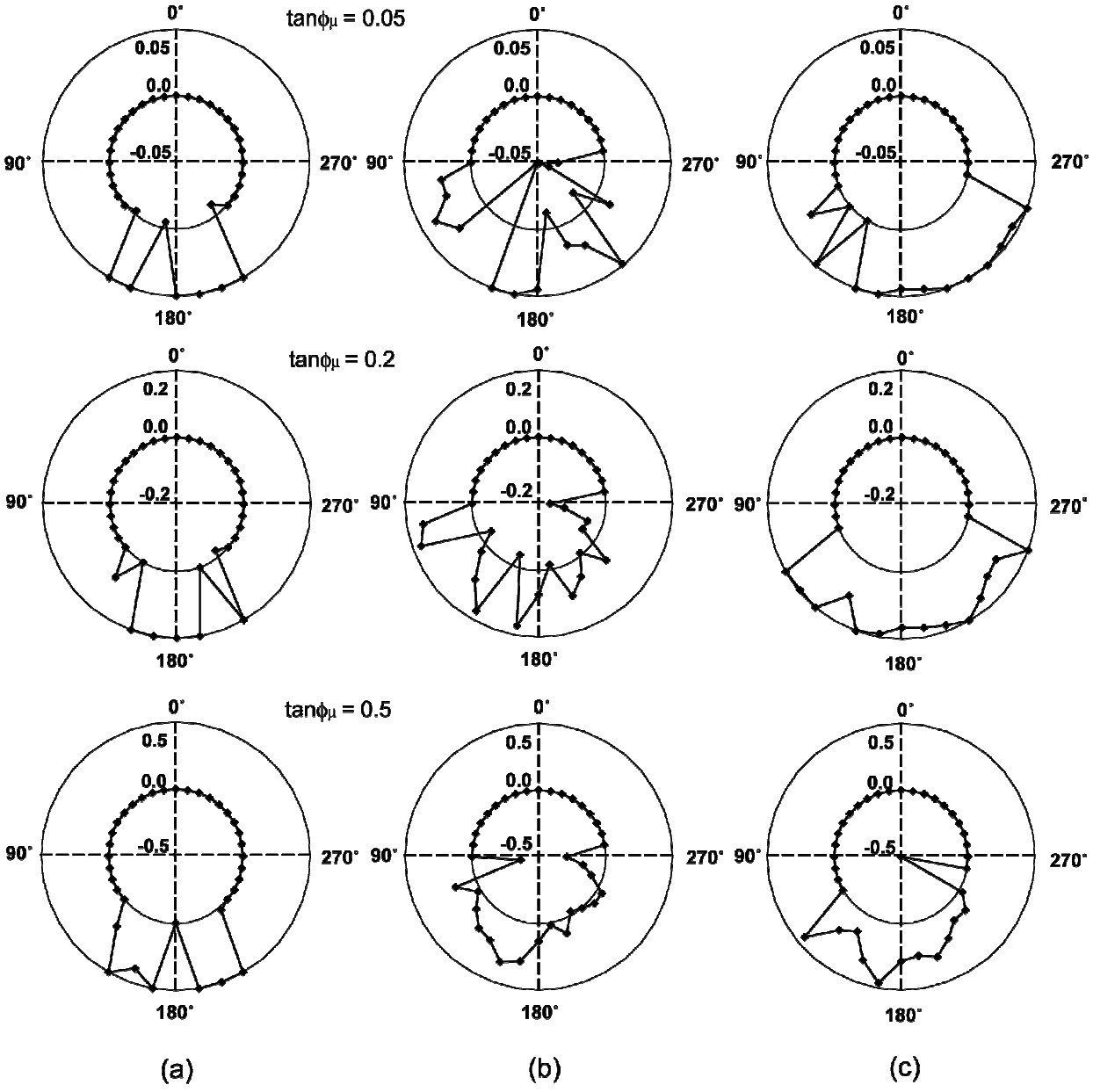

Figure 5.6. Mobilization of interface friction coefficient between particles and surfaces: (a) $R_t/D_{50} = 1$, Group 1; (b) $A_u/D_{50} = 4$ and $A_r = 2$, Group 4; (c) coextruded geomembrane surface, Group 5.

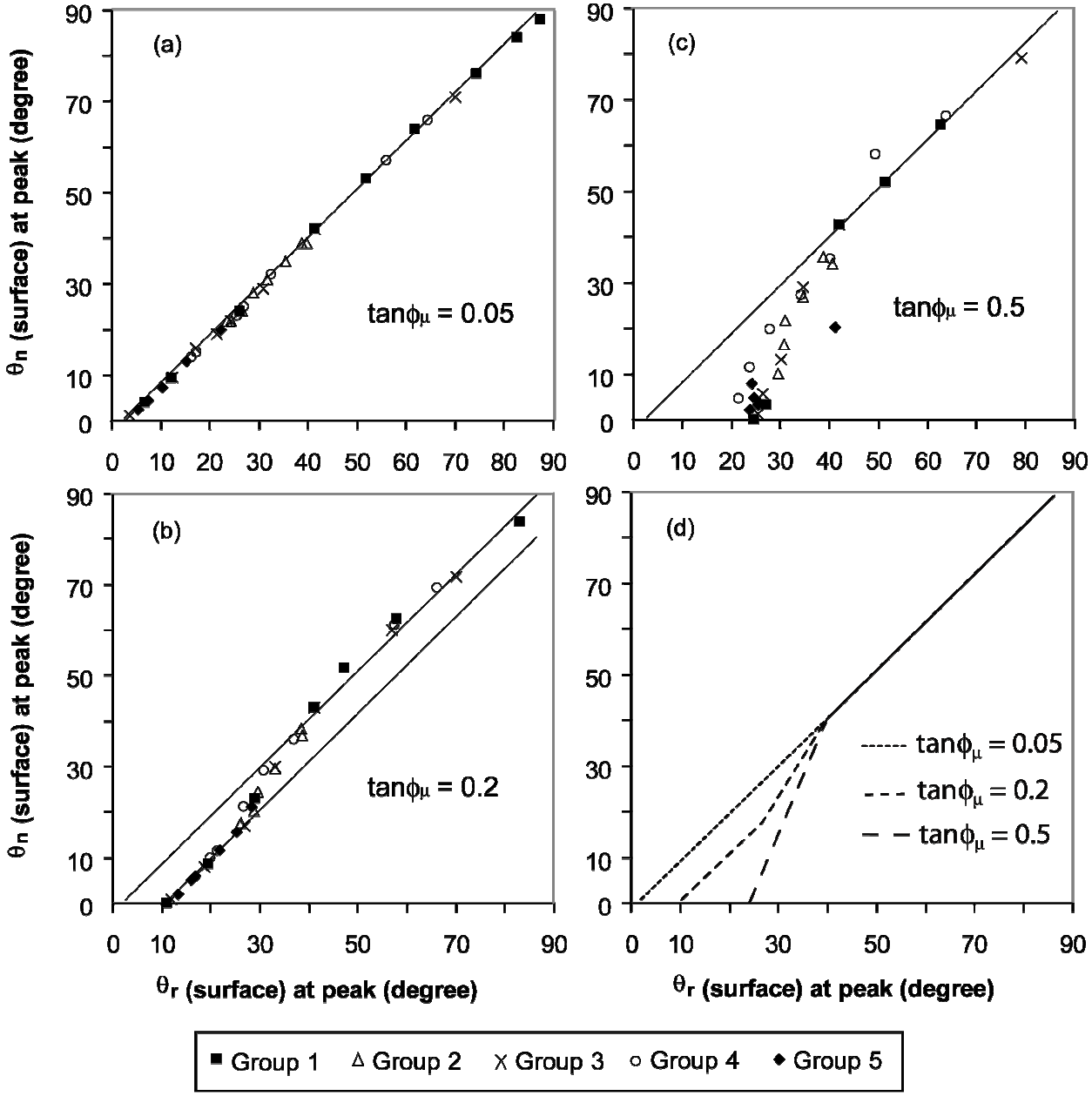

Figure 5.7. Relationships between of principal directions θ_n and θ_r under different ϕ_μ values: (a) $\tan\phi_\mu = 0.05$; (b) $\tan\phi_\mu = 0.2$; (c) $\tan\phi_\mu = 0.5$. Principal directions deviate from one another at high particle to surface friction coefficients and for surfaces causing low mobilization of granular material strength. As the surface mobilizes full granular material strength there is no difference between the average normal force and resultant force principal directions.